DELAMINATIONS UNDER PURE MODE II LOADING SHOW SIGNIFICANT LOCAL MODE I BEHAVIOUR

Isabelle Paris and Anoush Poursartip

Composites Group, Department of Metals and Materials Engineering,
The University of British Columbia, Vancouver, B.C., Canada, V6T 1Z4
http://www.composites.ubc.ca/

SUMMARY: In order to study delamination crack tip behaviour, several specimens have been tested under pure mode II loading inside a scanning electron microscope. One of the most interesting findings is the presence of crack opening displacements, even though the global loading has been independently confirmed to induce only pure shear. *COD* profiles have been measured for different applied mode II strain energy release rate values and their magnitude is very significant. The local crack opening is the result of the crack faces being moved apart as surface features slide over each other, and therefore the amount of opening varies with the surface roughness. For this reason, there is less opening when the crack is grown from an insert than when it has already been grown beyond the insert. Moreover, the variability in the amount of mode I opening can explain the higher scatter in G_{IIc} data in the literature.

KEYWORDS: fracture mechanics, delamination, in-situ, crack tip behaviour, crack opening displacement, crack shear displacement, scanning electron microscope (SEM)

INTRODUCTION

The topic of delamination growth has received much attention, with Linear Elastic Fracture Mechanics (LEFM), and in particular the strain energy release rate (G), being the most common approach to characterize the behaviour of a crack. Typically, knowledge of the global applied conditions (loads and/or displacements) and the geometry is used to calculate local parameters (G or the stress intensity factor K). However, local perturbations such as resin rich regions, fibre bridging and crack face waviness have been noticed by many investigators [1]. Thus global applied loads are often not transposed directly and uniquely into equivalent local crack tip conditions. Moreover, there is sometimes disagreement on how to partition modes in a mixed-mode loading case [2], and considerable controversy about the exact nature of mixed-mode fracture behaviour. Therefore, the objective of this work is to measure the load and displacement applied to a specimen and, at the same time, the crack tip behaviour, in order to establish a quantitative relation between them.

EXPERIMENTAL METHOD

A technique for measuring the local strain energy release rate based on the crack opening displacements (*COD*) and crack shear displacements (*CSD*) profiles at a delamination crack tip has been developed and is presented in [3,4]. The measured local strain energy release rate is compared to the global one, calculated from the globally applied conditions LEFM. The technique requires the use of an instrumented loading jig designed to fit inside a scanning electron microscope (SEM). Mode I, mode II and mixed-mode loading can be applied to a full size DCB specimen. The applied loads and displacements are measured and the images obtained simultaneously from the SEM are stored. After the test, crack opening (*COD*) and shear displacements (*CSD*) are measured on the images and compared to the ones predicted for the global strain energy release rate calculated from the applied loads and displacements using LEFM. A gold grid deposited on the edge of the specimen is used to provide reference points for the *COD* and *CSD* measurements.

The loading system has been tested to confirm that only a bending load is applied when a pure mode II loading condition is desired. A specimen was instrumented with two strain gauges close to the clamping point, on both surfaces, and loaded up to 100 N in mode II. The axial strain was less than 1% of the bending strains. The test was repeated several times, confirming that the loading was indeed pure mode II.

For an orthotropic DCB specimen under mode I or mode II load, the expression for the strain energy release rate has been obtained using finite element analysis in conjunction with analytical considerations [4,5]. We call them G_{IG} and G_{IIG}, to indicate that they are calculated from the global values. For the results presented in this paper, G_{IG} is always zero and the equation for G_{IIG} is:

$$G_{IIG} = \frac{9P_{II}\delta_{II}a^2\left(1+Y_{II}(\rho)\lambda^{-1/4}\frac{h}{a}\right)^2}{4EB^2h^3C_0 + 2B\left(L^3+3a^3\left(1+Y_{II}(\rho)\lambda^{-1/4}\frac{h}{a}\right)\right)} \tag{1}$$

$$\lambda = \frac{a_{11}}{a_{22}} \tag{2}$$

$$\rho = \frac{a_{12}+\frac{a_{66}}{2}}{\sqrt{a_{11}a_{22}}} \tag{3}$$

$$Y_{II}(\rho) = 0.206 + 0.078(\rho-1) - 0.008(\rho-1)^2 \tag{4}$$

where a_{ij} are the plane stress elastic compliance constants for the laminate: $a_{11} = \frac{1}{E_1}$, $a_{22} = \frac{1}{E_2}$, $a_{12} = \frac{-\nu_{12}}{E_1}$, $a_{66} = \frac{1}{G_{12}}$; a is the crack length, B is the specimen width; h is the specimen half-thickness; E is the laminate flexural modulus, C_0 is the machine compliance as determined experimentally [4].

The crack face displacements in an orthotropic material can be related to the strain energy release rate [6]. In this paper, we are interested in *COD* profiles. Eqn 5 is used to evaluate the local values of G_I that gives the best fit to the *COD* profiles measured experimentally on the SEM images. This value is called G_{IL} to indicate that it is calculated from the local crack tip conditions.

$$G_{IL} = \frac{\pi}{16\sqrt{2a_{11}a_{22}}}\left[\frac{2a_{12}+a_{66}}{2a_{11}}+\sqrt{\frac{a_{22}}{a_{11}}}\right]^{-\frac{1}{2}}\frac{COD^2}{r} \tag{5}$$

where r is the distance behind the crack tip.

TEST DESCRIPTION

Results are presented for 20 applied G_{IIG} levels distributed over 5 crack lengths and three DCB specimens of 24 layer unidirectional AS4/3501-6 CFRP laminate. The specimens dimensions are described in Table 1.

Table 1: Characteristics of specimens A, B and C.

	Specimen A	Specimen B	Specimen C
material	AS4/3501-6	AS4/3501-6	AS4/3501-6
V_f (%)	59	59	59
grid spacing (μm)	50.8	12.7	12.7
h (mm)	1.82	1.79	1.80
B (mm)	19.93	19.51	19.63
L (mm)	70.0	70.0	70.0
a (mm)	18.4 (A_{insert}) 19.0 (A_1) 23.3 (A_2)	18.4 (B_{insert})	44.64 (C_1)

A specimen with an insert, A_{insert}, was first loaded to G_{IIG} levels of 122 and 225 J/m^2 and unloaded. The crack was grown 600 μm from the insert under mode I loading and then loaded at G_{IIG} levels of 225 and 550 J/m^2 (A_1). The crack was extended 4.9 mm from the insert and loaded at the following G_{IIG} levels: 269, 324, 432, 543, 648 and 770 J/m^2 (A_2). Finally, the crack was loaded up to failure, which occurred at a G_{IIG} of 880 J/m^2.

A specimen (B_{insert}) was loaded, from the insert, to G_{IIG} levels of 104, 297, 494 and 695 J/m^2. Unstable crack growth occurred at 978 J/m^2. This specimen was used to study the effect of loading from the insert by comparing the results from tests from the insert (A_{insert} and B_{insert}) with the ones with a grown crack (A_1, A_2 and C_1).

A specimen (C_1) with a long crack grown in mode I (a=44.64 mm) was loaded at G_{IIG} levels of 103, 306, 499, 603 and 721 J/m^2. Then, unstable crack growth occurred, at a G_{IIG} of 833 J/m^2. This specimen was used to study the effect of a large starter crack on the crack tip behaviour.

For all tests, slow scan images from the SEM are recorded at the indicated G_{IIG} levels, at a magnification of 500x and a resolution of 1024 x 840 pixels. After the test, these images are

assembled in a montage: a typical image is shown in Fig. 1. From these images, the *COD* and *CSD* versus *r* profiles are obtained.

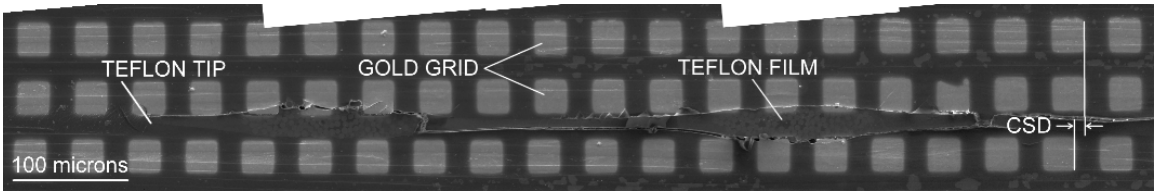

Fig. 1: SEM crack tip image (A_{insert}) for G_{IIG}=225 J/m^2

RESULTS

On all three specimens, matrix microcracks are formed ahead of the crack tip in the resin rich region between the fibres as mode II is applied, as has been reported in References [7,8]. These microcracks form at a 45° angle to the fibre direction, which is the plane of principal normal stress for a pure mode II loading. Between any two adjacent microcracks a ligament is created. As the mode II load is increased, the angle between the microcracks and the fibre direction increases. Finally the microcracked zone grows by coalescence of the microcracks at the fibre/matrix interface, either at the top or bottom of the matrix region. All these findings are in agreement with studies found in the literature [7,8,9].

The *COD* profiles were measured for the indicated G_{IIG} levels and crack lengths for specimen A (Fig. 2 and Fig. 3), B (Fig. 4) and C (Fig. 5). Since the crack tip position is changing due to microcracking, the *COD*s are plotted as a function of *x*, the position along the crack tip from an arbitrary origin, the same for all load levels.

For a pure mode II test, the *CODs* are expected to be 0. However, as can be seen in Fig. 2 to 5, a significant amount of local mode I opening is present. Careful observation of the SEM images shows that the crack is neither straight nor smooth. Thus the mode II shear loading of the crack forces the crack faces apart as the crack surface features slide over each other (Fig. 6). In other words, the local asymmetric crack topography combines with the pure shear applied globally to induce a local mode I loading.

The magnitude of this effect can be calculated from the *COD* measurements using Eqn 5. The values obtained for G_{IL} are indicated on Fig. 2 to 6 beside each dashed line profile. We notice that the measurements agree well with a square root singularity for a length of roughly 1 mm from the crack tip. Then the *COD*s seem to reach a plateau. This can be explained by the fact that, at a certain distance behind the crack tip, a maximum surface roughness has been reached and the height of these bumps is roughly constant.

In Fig. 2 to 5, we can also see that, for the lower applied G_{IIG} loads, the *COD* profiles have the same origin with increasing mode II load, since the ligaments created by the microcracking can still withstand an opening load. However, at higher load levels, for A_1, A_2 and C_1, the origin of the *COD* profile is shifting: the crack is advancing because the microcracks are coalescing. Visual observation of the images confirms that the distance obtained from the shift in the *COD* profiles agrees very well with the length of the coalesced zone. There is practically no coalescence for A_{insert} and B_{insert}.

In Fig. 3, it can be seen that initially, with no mode II load, a mode I component of roughly 5 J/m^2 is present. Since the crack has been grown 4 mm from the insert, there is debris preventing it from shutting closed.

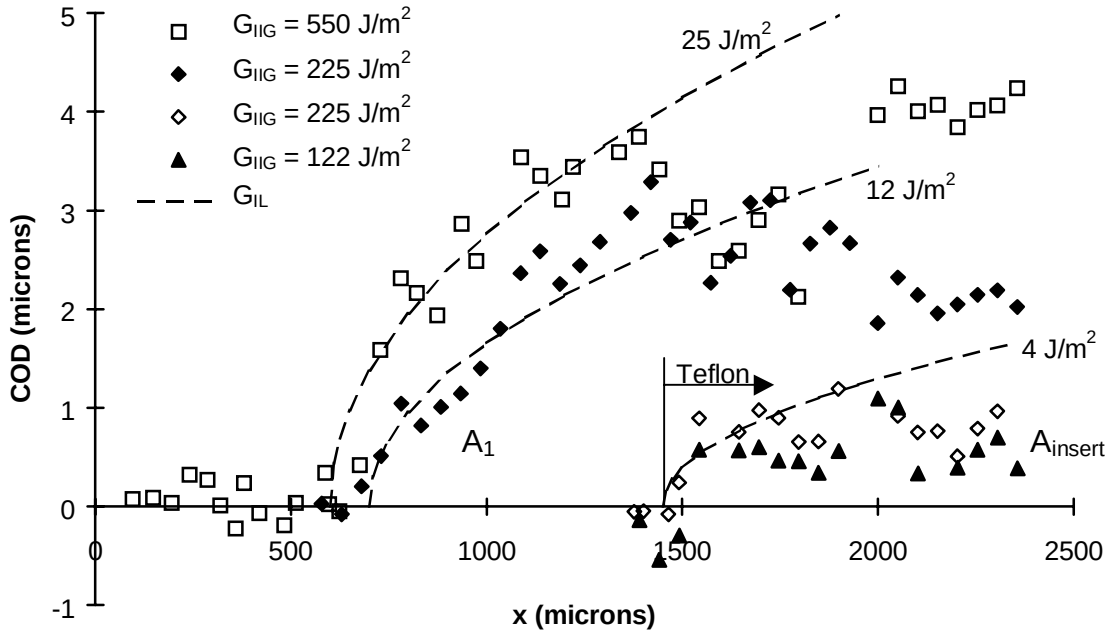

Fig. 2: Plot of COD vs. x (distance from the crack tip) for specimen A (A_{insert} and A_1) loaded under pure mode II. Dashed lines show COD profiles for G_{IL} that best fit the measurements.

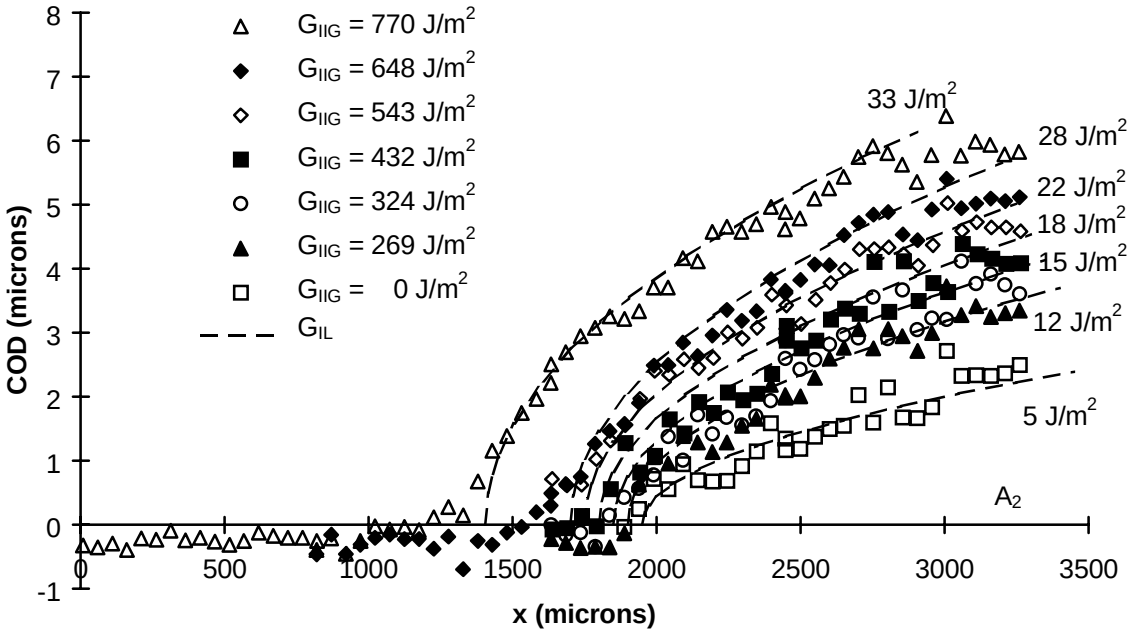

Fig. 3: Plot of COD vs. x (distance from the crack tip) for specimen A_2 loaded under pure mode II. Dashed lines show COD profiles for G_{IL} that best fit the measurements.

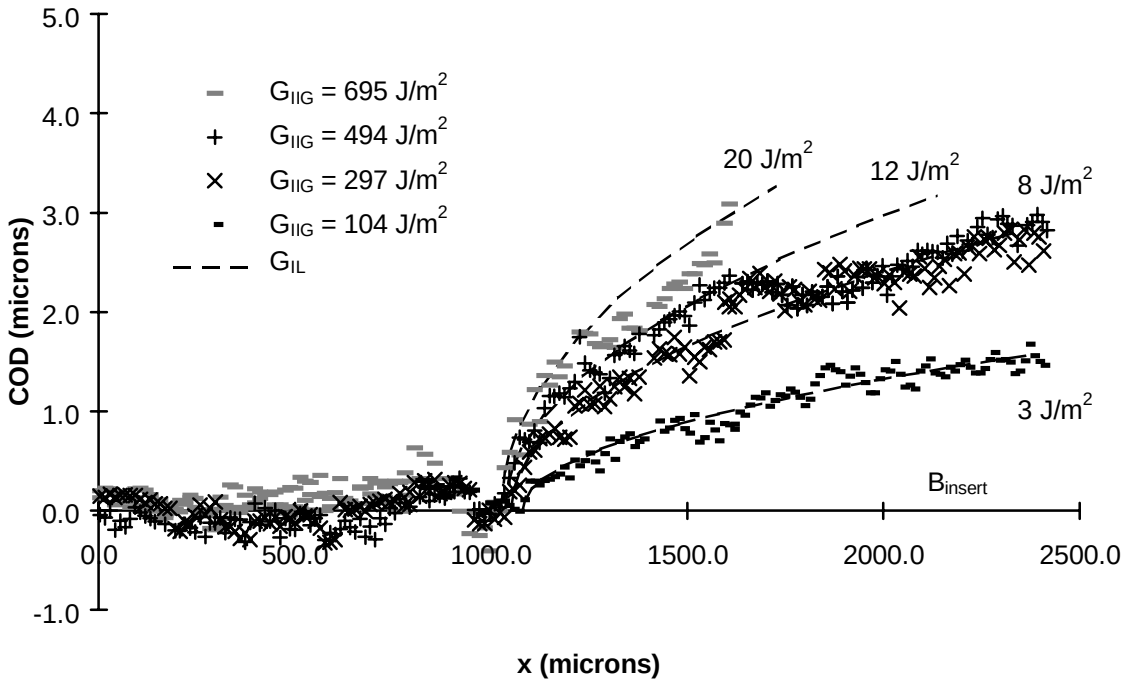

Fig. 4: Plot of COD vs. x (distance from the crack tip) for specimen B_{insert} loaded under pure mode II. Dashed lines show COD profiles for G_{IL} that best fit the measurements.

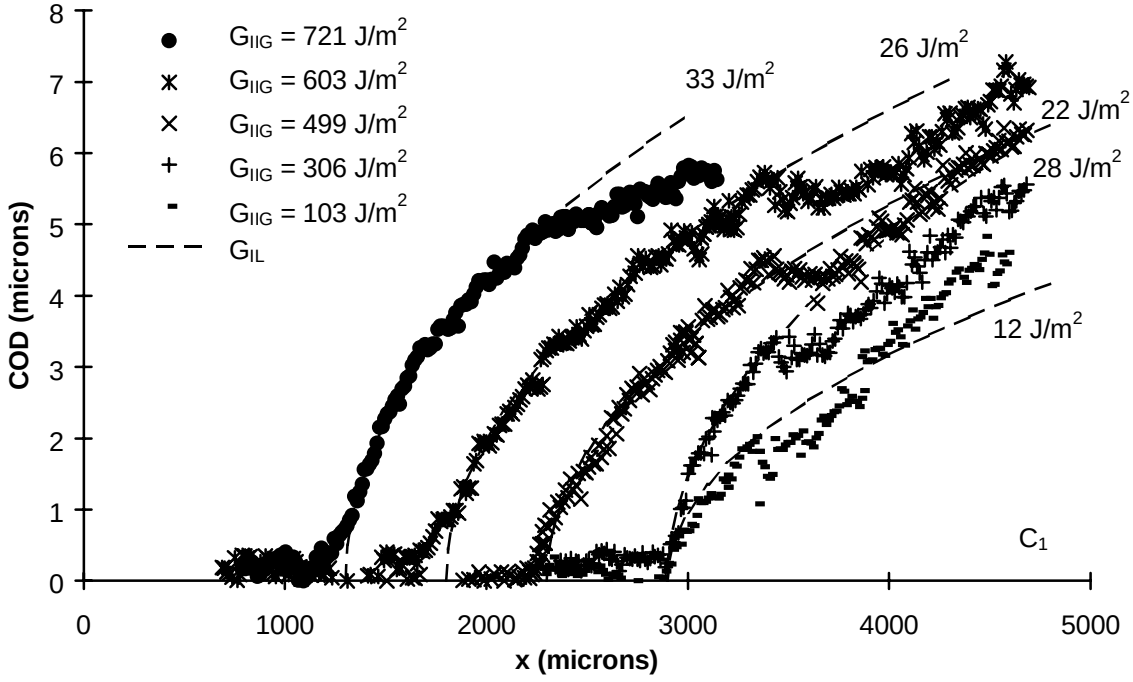

Fig. 5: Plot of COD vs. r (distance from the crack tip) for specimen C_1 loaded under pure mode II. Dashed lines show COD profiles for G_{IL} that best fit the measurements.

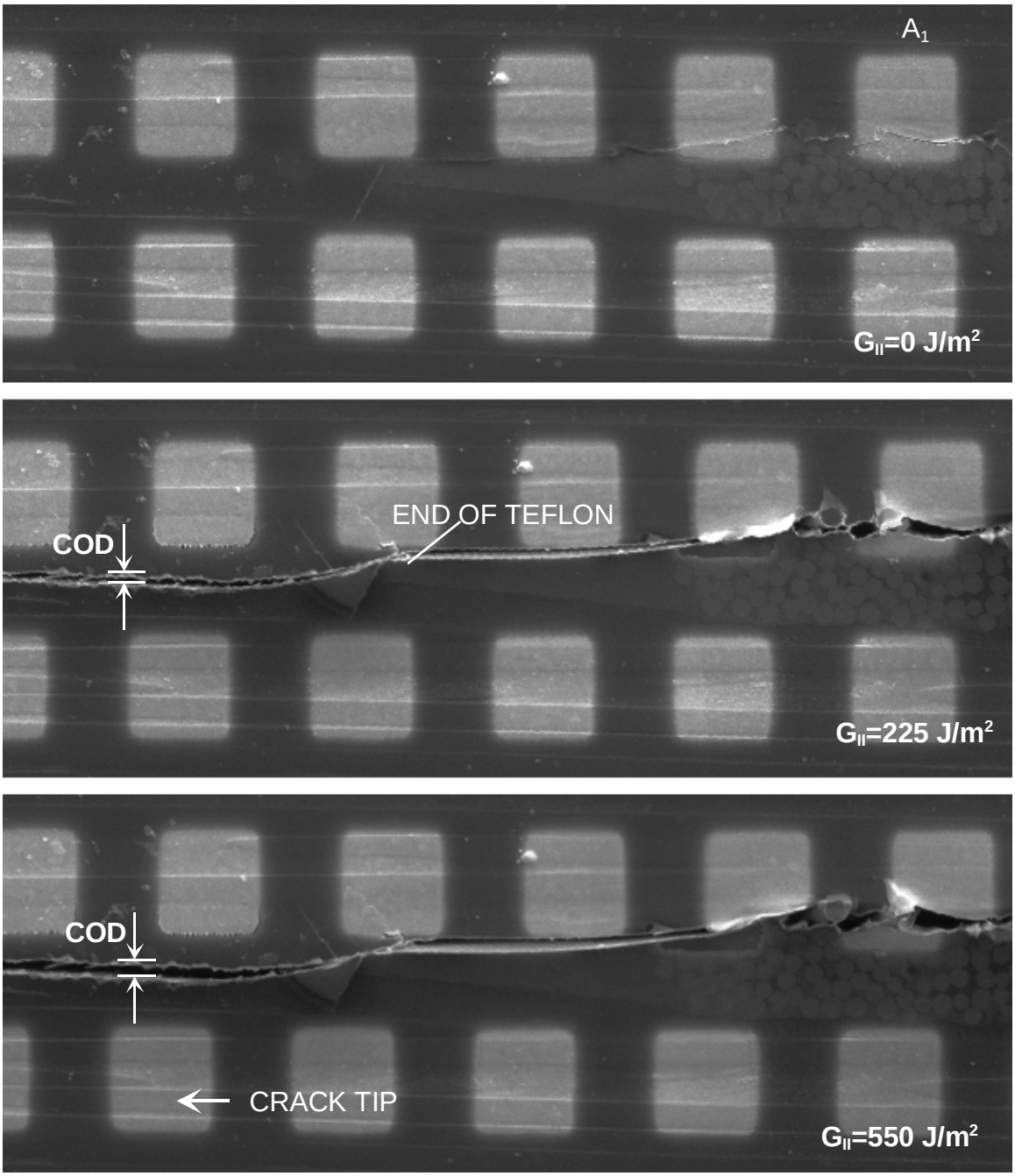

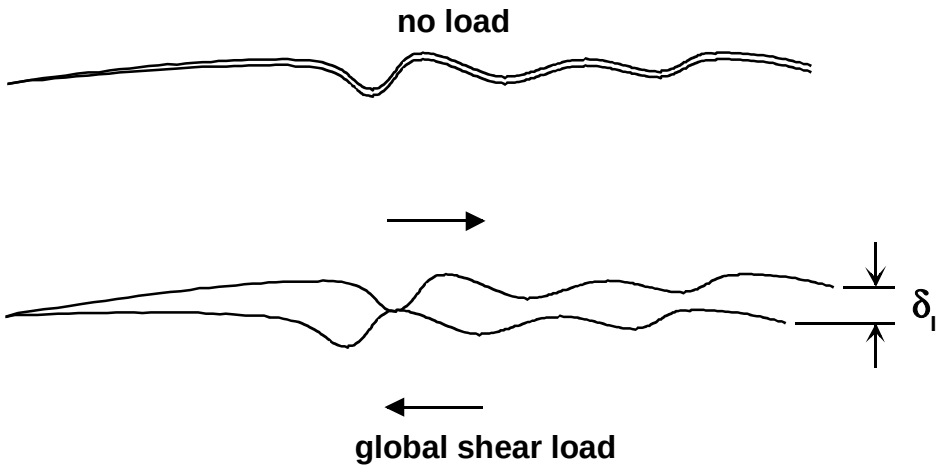

Fig. 6: Local opening displacement created under global shear loading

Relation between mode I and mode II

For all the specimens, the magnitude of the *COD*s increases with the mode II load, as the wavy crack surfaces slide over each other. As can be seen in Fig. 7, where G_{IL} is plotted against G_{IIG}, the magnitude of G_{IL} increases with the applied mode II loading, as would be expected from the proposed mechanism. When there is only an insert (A_{insert} and B_{insert}), G_{IL} is much smaller for the same G_{IIG}. This can be explained by the fact that the Teflon insert is smoother than the crack grown in the material. Furthermore, since G_{IL} is lower, the ligaments are less likely to reach the limit strain. This can therefore explain why the microcracks are not coalescing, as mentioned previously.

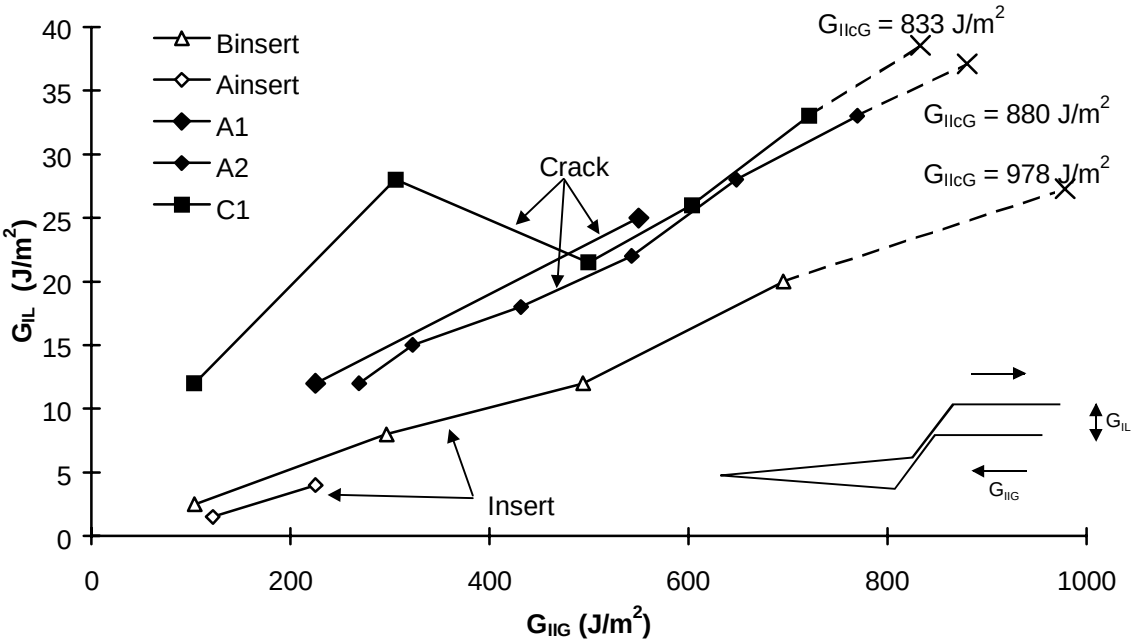

Fig. 7: Plot of G_{IL} vs. G_{IIG} global for specimen A, B and C. Hollow markers indicate tests from an insert. The x markers show values at failure (G_{ILc} evaluated by linear extrapolation).

G_{IL} values as high as 33 J/m^2 are measured: this is 25% of G_{Ic}, and therefore the mode I component is very significant. Moreover, these high G_{IL} values are measured before unstable failure is reached: G_{IL} at failure is likely to be even higher. Thus final failure in what is nominally a pure mode II test may be influenced significantly by the mode I component. In Fig. 7, the G_{IL} values at failure have been evaluated by linear interpolation and plotted against G_{IIcG} (dashed lines) for the 3 cases were G_{IIcG} is known. Even though these values are not exact, they show a trend: the higher the measured G_{IIcG}, the lower the measured mode I component. This would confirm the findings by several authors that G_{IIc} from an insert is higher than from a precrack [10], since, as we have now seen, G_{IL} is lower due to less surface waviness.

Fig. 8 shows the effect of not knowing that there is a mode I component on the mixed-mode failure envelope, for the 3 failure points shown in Fig. 8. The pure mode I value comes from a specimen loaded under pure mode I [4]. If we neglect the mode I component, the G_{IIc} values are different and there seems to be significant scatter in the data. If the G_{IL} values are included, then each data point is shifted up by a different amount and there is a linear relation between them, rather than scatter. Interestingly, O'Brien [10] points out that the scatter in mixed-mode delamination test results for AS4/3501-6 increases significantly for high mode II.

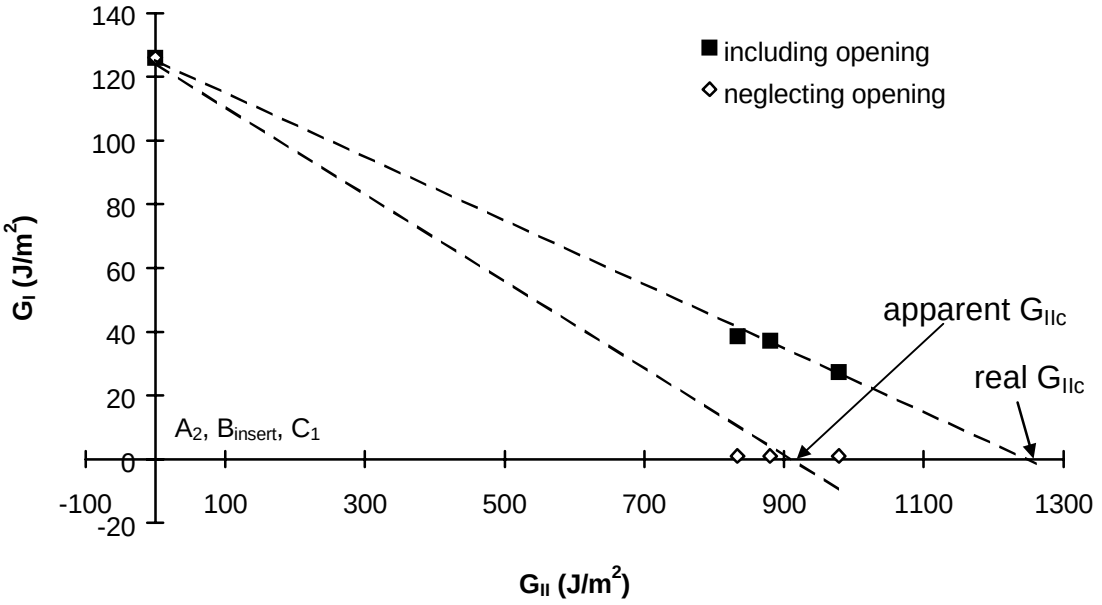

Fig. 8: Effect of neglecting the mode I opening due to surface waviness on the mixed-mode failure envelope.

CONCLUSION

Several specimens have been tested, showing that under nominally pure mode II loading, the crack tip is opening in mode I. This is due to the face roughness, which forces the crack tip open as surface features slide over each other. The amount of opening varies with the waviness of the crack. For example, the local mode I opening is lower when the crack tip is at the end of an insert than when the crack grows beyond the insert. This could partly or wholly explain why initiation G_{IIc} values are found to be higher than propagation values.

The variable nature of surface waviness, and therefore, the variable amount of local mode I opening, can also explain the large scatter observed by many investigators in G_{IIc} data, as the tests are not really pure mode II tests, but in fact mixed-mode tests with unknown and variable proportions of mode I. The determination of the widely quoted mode II material toughness is therefore open to question. The work presented here should be considered in the development of a standard pure mode II test for the determination of G_{IIc}. More generally, this work also suggests that mixed mode loading might result in local crack tip conditions quite different than predicted from the partitioning of globally applied loads, with considerable effect on mixed mode failure envelopes.

AKNOWLEDGMENTS

This work was supported by funding from the Defense Research Establishment Pacific, the Natural Sciences and Engineering Research Council of Canada and the Fonds pour la Formation de Chercheurs et l'Aide à la Recherche. We would like to gratefully acknowledge the interaction and support from our colleagues at The University of British Columbia. In particular, we would like to thank Roger Bennett, Mary Mager, Serge Milaire and Ross McLeod for their assistance in developing the experimental set-up.

REFERENCES

1. Davies, P. and Benzeggah, M.L., "Interlaminar Mode-I Fracture Testing", *Application of Fracture Mechanics to Composite Materials*, K. Friedrich, Ed., Elsevier Science Publishers, Amsterdam, 1989, pp. 81-112.

2. Hashemi, S., Kinloch, A. and Williams, G., "Mixed-Mode Fracture in Fiber-Polymer Composite Laminates", *ASTM STP 1110*, American Society for Testing and Materials, Philadelphia, 1991, pp. 143-168.

3. Paris, I. and Poursartip, A., "Delamination Crack Tip Behaviour at Failure in Composite Laminates under Mode I Loading", *Journal of Thermoplastic Materials*, Vol. 11, 1998, pp. 57-69.

4. Paris, I., "In-Situ Measurements of Delamination Crack Tip Behaviour in Composite Laminates inside a Scanning Electron Microscope", Ph.D. thesis, The University of British Columbia, Vancouver, BC, Canada, 1998.

5. Hutchinson, J.W. and Suo, Z., "Mixed Mode Cracking in Layered Materials", *Advances in Applied Mechanics*, Vol. 29, 1992, pp. 63-191.

6. Poursartip, A., Gambone, L.R., Ferguson, J.S., et al, "In-Situ SEM Measurements of Crack Tip Displacements in Composite Laminates to Determine G in Mode I and Mode II", *Engineering Fracture Mechanics*, Vol. 60, No. 2, 1998, pp. 173-185.

7. Hibbs, M.F. and Bradley, W.L., "Correlations Between Micromechanical Failure Processes and the Delamination Toughness of Graphite/Epoxy System", *Fractography of Modern Engineering Materials: Composites and Metals, ASTM STP 948*, Masters, J.E., and Au, J.J., Ed., American Society for Testing and Materials, Philadelphia, 1987, pp. 68-97.

8. O'Brien, T.K., Murri, G.B. and Salpekar, S.A., "Interlaminar Shear Fracture Toughness and Fatigue Thresholds for Composite Materials", *Composite Materials: Fatigue and Fracture (Second Volume), ASTM STP 1012*, Lagace, P.A., Ed., American Society for Testing and Materials, Philadelphia, 1989, pp. 222-250.

9. Russell, A.J. and Street, K.N., "Moisture and Temperature Effects on the Mixed-Mode Delamination Fracture of Unidirectional Graphite/Epoxy", *Delamination and Debonding of Materials, ASTM STP 876*, Johnson, W.S., Ed., American Society for Testing and Materials, Philadelphia, 1985, pp. 349-370.

10. O'Brien, T.K., "Composite Interlaminar Shear Fracture Toughness, G_{IIc}: Shear Measurement or Sheer Myth?", Technical Memorandum, NASA TM-110280, NASA Langley Research Center, 1997.